©Copyright 2017
Peter T. Vonich

Hurricane kinetic energy spectra from in situ aircraft observations

Peter T. Vonich

A thesis
submitted in partial fulfillment of the
requirements for the degree of

Master of Science

University of Washington

2017

Committee:

Gregory Hakim, Chair

Dale Durran

Clifford Mass

Program Authorized to Offer Degree:
Department of Atmospheric Sciences

University of Washington

Abstract

Hurricane kinetic energy spectra from
in situ aircraft observations

Peter T. Vonich

Chair of the Supervisory Committee:
Dr. Gregory Hakim
Department of Chair

Just over 30 years ago, Nastrom and Gage (1985) completed their seminal paper on aircraft-derived power spectra. Since then, significant strides have been made in understanding the wavenumber distribution of energy in Earth's atmosphere and its implications on the mathematical limits of forecasting. In recent decades, the meteorological community has enjoyed a substantial degree of success in improving forecast skill, but hurricane intensity predictions have persistently lagged behind. Limited intrinsic predictability is believed to be partially responsible for the failure to appreciably increase tropical cyclone (TC) intensity skill. In this study, aircraft data is analyzed from over 1200 missions carried out by the National Oceanic and Atmospheric Administration (NOAA) and Air Force Reserve Command (AFRC) Hurricane Hunters. Each mission is parsed into distinct flight legs, and legs meeting a specified set of criteria are retained for spectral analysis. Power spectra composites for each category of the Saffir-Simpson scale are produced and reveal relationships between spectral slope and intensity. As hurricane intensity increases, it is found that 1) spectral slope becomes steeper across scales from 10 km to 160 km and 2) the transition zone where spectral slope begins to steepen in value (usually about 400 km; Nastrom and Gage 1985) shifts downscale. Possible explanations for steepening spectral slope and shifting transition zone are briefly postulated as the product of strong rotation.

TABLE OF CONTENTS

LIST OF FIGURES

ACKNOWLEDGMENTS

This study was supported by the NSF Graduate Research Fellowship Program (2015199752) and the NOAA HFIP (NA14NWS4680031). Thank you to Neal Dorst, Jack Parrish, Ashley Lundry, Sonia Otero, and Sim Aberson for information regarding data formatting and flight procedures. A special thanks to the crews of the AFRC and the NOAA Hurricane Hunters, without whom this research would never have been possible. Finally, many thanks to the University of Washington.

DEDICATION

To my dad, Pete.

The original inspiration to my passion for meteorology.

Rise above.

Chapter 1

INTRODUCTION

The ongoing struggle to improve hurricane intensity forecasts has become somewhat of an atmospheric cliché in the meteorological community. Error trends for lead times greater than 24 hours have trended slightly downward, but despite the substantial success seen in reducing average hurricane track error, hurricane intensity skill has remained more or less stagnant.

The challenge of enhancing TC wind speed forecasts is thought to involve several levels within the modeling chain. Rogers et al. (2013) succinctly summarized the issues in their aircraft-based TC investigation, stating that the TC intensity skill shortfall exists within microphysical processes and predictability constraints. Recent research connected with the Hurricane Aerosol and Microphysics Program (HAMP)–a sister project to the Hurricane Forecast Improvement Project (HFIP)–has shed some light on the importance of microphysical processes to intensity forecasting (see Rosenfeld et al. 2007; Khain et al. 2010; Rosenfeld et al. 2011), but considerable research is needed. This is especially true with regards to the fundamental forecasting limitations imposed by TC predictability.

The study of atmospheric predictability revolves around the growth of errors. Given the power spectrum of a fluid flow, conclusions can be drawn as to how quickly small scale errors will contaminate large scales. Lorenz (1969) was the first to demonstrate this relationship, spurring research into the field of atmospheric predictability which continues today. He demonstrated that for a given flow, scales governed by a k^{-p} power-law (where $p < 3$) have limited predictability while scales governed by $p \geq 3$ have unlimited predictability. At the time of publication, Lorenz (1969) had only considered the predictability of flows within the two-dimensional vorticity (2DV) equation framework. Rotunno and Snyder (2008)

apply Lorenz's spectral model to the surface quasi-geostrophic equations (SQGs) to relax 2DV's inability to capture essential baroclinic effects. Their work confirmed that the energy spectrum of a basic flow influences predictability far more than the dynamical framework (2DV or SQG) under which it is applied.

Although Lorenz had laid the theoretical foundation for the predictability of flows, little data existed in 1969 by which to test his theory to the actual atmosphere. That all changed following the 1975 to 1979 NASA-led Global Atmospheric Sampling Program (GASP). During this program Boeing 747s fitted with special instrumentation gathered atmospheric data along commercial flight paths, providing Nastrom and Gage (1985) with the data to complete their seminal paper on wind and temperature wavenumber spectra. Their study yielded a power spectrum with a $k^{-5/3}$ power-law for wavelengths less than 400 km and a k^{-3} relationship for wavelengths larger than 400 km. These findings dispelled theories that–at the time–proposed a mesoscale energy gap. The continuous increase in energy from small to large scales demonstrated by Nastrom and Gage (1985) corroborated the findings of Lilly and Petersen (1983) and displayed consistency with Vinnichenko (1970), Balsley and Carter (1982), and Chen and Wiin-Nielsen (1978). Though the impact of Nastrom and Gage (1985) on the atmospheric sciences can hardly be overstated, it only offers a general description of Earth's wind and temperature spectra. Would Nastrom and Gage's spectrum be representative of a conditional atmospheric environment such as that found in a TC?

The goal of this paper is to begin exploring that question, utilizing in situ aircraft observations to generate power spectra for hurricanes. Just as Nastrom and Gage created a climatology of wavenumber spectra for the upper troposphere, we have computed a collection of TC wavenumber spectra for each category of the Saffir-Simpson scale. For the remainder of the paper, we describe how the Hurricane Hunters acquire their data in Section 2, discuss our methods for generating TC spectra in Section 3, present intriguing spectral slope results in Section 4, and summarize our findings and future work in Section 5.

Chapter 2

DATA

2.1 AFRC and NOAA Hurricane Hunters

Every hurricane season, the NOAA Hurricane Hunters fly WP-3D aircraft out of MacDill Air Force Base (AFB), Florida to conduct atmospheric reconnaissance missions in the Atlantic Basin and Eastern North Pacific. The United States AFRC operates their own hurricanes hunting unit, the 53rd Weather Reconnaissance Squadron (53WRS), flying WC-130s out of Keesler AFB, Mississippi. During missions, aircraft-mounted instruments record wind speed (± 4 knots), wind direction (± 10 degrees), GPS position (± 3 nautical miles), temperature, dew point, mixing ratio, altitude, and other variables (National Hurricane Operations Plan). The data gathered by these units serves to augment and verify TC track and intensity forecasts.

Missions analyzed during this study can be separated into 3 datasets: 1) NOAA data, 2) AFRC 1 second (s) data, and 3) AFRC 10 s data. For flights occurring from 1960 to 2009, AFRC wind data is available at 10 s intervals, where each wind value represents a trailing average of the wind speeds measured during each of the previous 10 s (Weather Bird Software Logic and Algorithms). After 2009, the 53WRS upgraded to 1 s data output. Each wind value in the AFRC 1 s dataset represents a 30 s average of the wind speeds taking place during the 15 seconds before and after a specified time (Weather Bird Software Logic and Algorithms). NOAA wind speed data is output at 1 s as well and represents the average wind speed during a given second, where wind speeds are measured at a rate faster than 1 Hertz (Hz). Both NOAA and AFRC wind data are adjusted for aircraft angle of attack and sideslip angle. Wind speeds are recorded at the nearest knot (kt) for the AFRC and the nearest tenth of a meter per second (m/s) for NOAA. Additional detail regarding data

Table 2.1: Collection of mission statistics and power spectra results organized by storm intensity.

Category	Missions	Flight Legs	Steepest Slope	Bin of Steepest Slope (km)	Mean Slope
Cat-5	43	274	-3.1	43-68	-2.2
Cat-4	120	760	-2.4	43-68	-2.0
Cat-3	114	718	-2.5	68-106	-2.0
Cat-2	146	922	-2.3	106-166	-1.8
Cat-1	274	1597	-2.1	68-106	-1.8
TS	583	2973	-1.9	43-68	-1.7

processing, data quality, and flight procedures can be found in the Appendix.

For this study, we utilize tropical storms (TS) and hurricanes from 1980 to 2015, beginning with Hurricane Allen and ending with Hurricane Patricia. After screening available missions for quality and relevance, 1280 missions were found suitable for analysis. These 1280 missions are spread across 217 named storms and a breakdown of their intensities is available later in Table 2.1. Older missions–particularly those from the 53WRS in the 1980s and 1990s–do not include aircraft speed data. Selection of suitable missions and calculation of power spectra in the absence of aircraft speed are addressed in Section 3c.

2.2 NOAA Best Track Data

Flight legs must pass through the radius of maximum wind (RMW) to be considered for spectral analysis. To make this determination, NOAA Best Track (NBT) data was employed (detailed explanation in Section 3b). Maximum 1-min surface wind speed, minimum central pressure, and storm position for North Atlantic and Eastern Pacific storms are logged every 6 hours by the NHC. The Joint Typhoon Warning Center (JTWC) accomplishes the same task for the West Pacific, South Pacific, South Indian, and North Indian. Occasionally the AFRC Hurricane Hunters travel to the West Pacific during the North Atlantic's dormant winter months, but the vast majority (greater than 99%) of storms evaluated during this study are from the North Atlantic and Eastern Pacific.

Chapter 3

METHODS

3.1 Selecting suitable missions

1280 missions are utilized in this study. In order to distill the available missions into a relevant set, a subjective screening method is applied. Mission GPS data are plotted and compared to NBT position data during the time of hurricane intercept. If the mission's flight pattern coincide with the storm position from the NBT data, then the storm is retained for further evaluation. Plotting the flight tracks exposes ferry, ocean wind survey, and synoptic surveillance flights. These missions do not involve hurricane intercepts so they are not analyzed. Missions are classified on the Saffir-Simpson scale based on the maximum sustained winds of the NBT data point closest to the intercept time. If NBT data is not available within 3 hours of a hurricane intercept, the mission is not analyzed.

3.2 Identifying flight legs

We are only concerned with power spectra of flight legs intersecting the RMW. To determine whether a flight leg has met this criterion, a mission's flight track is separated into legs (Fig. 1a). Hurricane intercept times do not correspond exactly to NBT records, so the position of a storm is linearly interpolated between the two closest NBT position points based on the time of intercept. A 0.25° (approximately 55 km)[1] radius circle is plotted around the storm center with the intention of simulating the RMW as seen in (Fig. 1b). Flight legs intersecting this circle are considered to have passed through the RMW.

---

[1]The average RMW for Cat-2, Cat-3, and Cat-4 storms was found by Hsu and Yan (1998) to be 48 km. Increasing this distance to 55 km radius allows for a small buffer given a storm's continual movement during a mission.

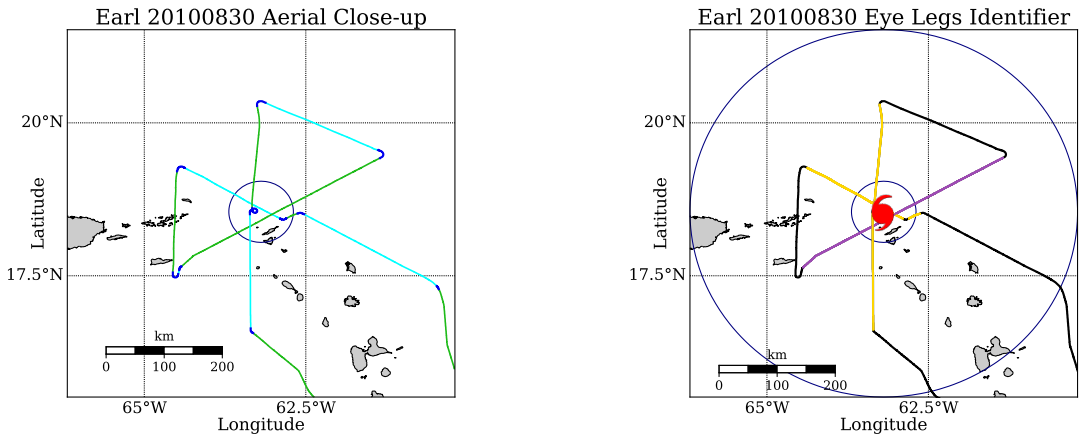

(a) (b)

Figure 3.1: Distinct flight legs are shown in 3.1(a) as light blue and green. An algorithm partitions the overall flight path into unique legs when a ground track variance threshold is exceeded, indicating a turn (shown in dark blue). Flight legs intersecting the 0.25° in 3.1(b) are highlighted in orange, with the purple leg corresponding to the velocity profile shown in Fig. 3.3.

3.3 Spectral analysis

After qualifying flight legs are determined, each leg is truncated at the RMW to exclude the sharp discontinuity occurring between the RMW and the eye of the storm. Fig. 3.2(a) illustrates this concept with a Rankine vortex (RV). We see in Fig. 3.2(b) that removing the sharp discontinuity in the RV velocity data eliminates spectral overshoot and other complications related to aliasing. Flight legs shorter than 10 km are not analyzed. This is due to wind speed variability, which makes it difficult to identify the RMW over short distances. Finally, if a flight leg extends across the full diameter of the storm, two new flight legs are created–one on each side of the RMW (see real world example in Fig. 3.3).

After a flight leg is truncated at the RMW, wind speeds are interpolated to a regular grid. Grid spacing for a flight leg is defined as the plane's average airspeed multiplied by the sampling interval (1 s or 10 s). Nastrom and Gage (1985) essentially operates under the assumption that Boeing 747 ground speeds (roughly 250 m/s) are large compared to

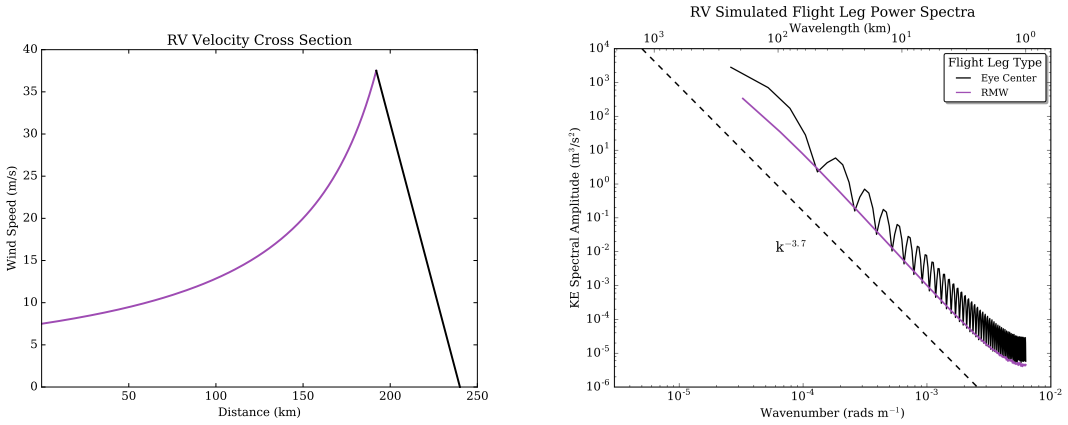

(a) (b)

Figure 3.2: A RV radial velocity profile is shown in Fig. 3.2(a) with the purple curve representing winds before RMW truncation, and the black curve showing the truncated portion of a hypothetical flight leg. Fig. 3.2(b) displays the power spectra of the retained wind data (purple) and the retained wind data plus the truncated information (black). Aliasing results in the black curve because the sharp discontinuity is not removed. The purple curve has a slope of approximately -3.7.

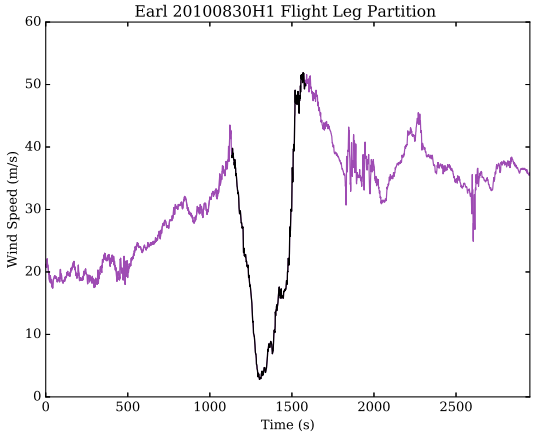

Figure 3.3: Wind data from a flight leg spanning the full diameter of Hurricane Earl on August 30, 2010 is truncated at the RMW similar to Fig. 3.2(a). The complete flight leg is separated into two smaller flight legs (purple), while the sharp discontinuities and eye (black) are removed.

the speed of relevant atmospheric disturbances–that is to say, disturbances move negligible distances during the time it takes to sample them. As a result, Nastrom and Gage (1985) simply prescribes wind values to a 250 m grid. Lilly and Petersen (1983) attempt to address the subtleties of relative motion between aircraft and disturbances by using mean airspeed (240 m/s). Understanding that no all-encompassing method could account for every nuance regarding relative motion, Lilly and Petersen conclude most resulting errors cancel out in the overall mean. Given the symmetric flight paths conducted by the 53WRS and NOAA, we draw the same conclusion, contending that any errors caused by relative motion cancel out in the overall mean. Moreover, TC winds are almost entirely azimuthal at aircraft flight levels. Consequently, ground speed and airspeed are virtually the same. As a result, we simply use ground speed to calculate the normalizing factor explained in the follower paragraph. AFRC 1 s missions occurring before 2005 (about 0.83% of all missions) do not contain ground speed or airspeed, so average ground speed is determined by flight leg length divided by time.

After interpolating wind speeds to a regular grid, the mean and endpoint-to-endpoint linear trend are removed. A Fast Fourier Transform (FFT) is applied and the squared Fourier coefficients are used to produce a periodogram for each flight leg (Fig. 3.4). Since each flight leg has a unique grid spacing and average speed, the spectral amplitudes of each periodogram are multiplied by the normalizing factor, $\frac{\Delta x}{\pi N}$, where Δx is distance between grid points, and N is the number of data points in a flight leg (Durran et al., 2017). After normalization, the spectral amplitudes in each periodogram are distributed across 17 logarithmically-spaced wavenumber bins in the same manner as Lilly and Petersen (1983) and the points within each bin are averaged to create a power spectrum composite for each category of the Saffir-Simpson scale. Four spectral composites are produced: a NOAA composite, an AFRC 1 s composite, an AFRC 10 s composite, and a joint composite comprised of all three datasets.

The maximum (minimum) wavenumber (wavelength) bin edge is 1×10^{-2} radians per meter (rads m^{-1}), 2×10^{-3} rads m^{-1}, and 2×10^{-3} rads m^{-1} for the NOAA 1 s, AFRC 1 s, and AFRC 10 s composites, respectively. Upper (lower) wavenumber (wavelength) bounds are set for the NOAA and AFRC 1 s datasets so as to discard wavenumbers affected by the moving

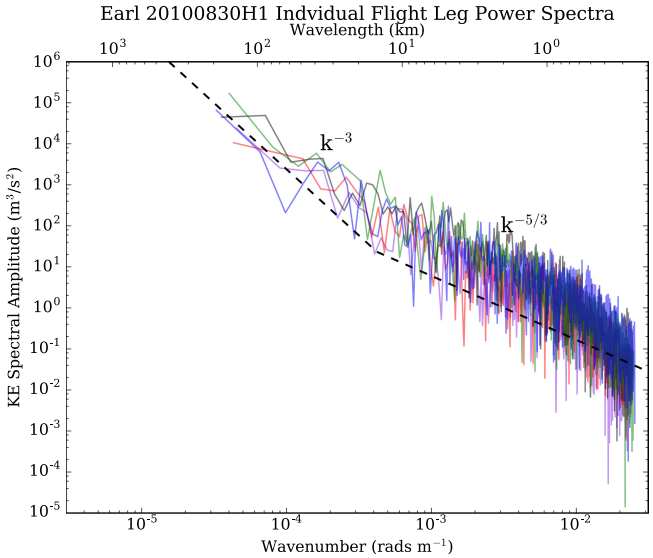

Figure 3.4: Periodograms corresponding to flight legs from the mission pictured in Fig. 1b. 7244 total periodograms (flight legs) are averaged to form the composite spectral profiles for each category of the Saffir-Simpson scale shown in 4.4. Dashed reference lines represent $k^{-5/3}$ and k^{-3} slopes.

averages mentioned in Section 2a. Though the AFRC 10 s data has no averaging concerns, 2×10^{-3} rads m^{-1} is chosen as the upper wavenumber bound in order to remove scales aliased at the Nyquist frequency. Finally, the combined dataset has an upper wavenumber bound of 1×10^{-2} rads m^{-1} (3.1 km) as defaulted by the bound applied to NOAA and a lower bound of 6.28×10^{-6} rads m^{-1} (1000 km) to remove highly variable spectra caused by the small number of flight legs greater than 1000 km. The NOAA, AFRC 1 s, and AFRC 10 s composites have no lower wavenumber bound.

Chapter 4

RESULTS

4.1 Power spectra composites

7244 flight legs are analyzed from a total of 1280 missions. 7148 of these flight legs are 1000 km in length or less, and 96 are greater than 1000 km (see Fig. 4.1). Leg truncation at the RMW tends to decrease the number of long flight legs, while increasing the number of short flight legs. Typical hurricane dimensions also tend to force the distribution away from the synoptic scales. The average storm latitude is 23.4° N with 97% of missions taking place in storms located between 10° N and 35° N. Like Lilly and Petersen (1983), the standard deviation of each bin population is about the same magnitude as the bin's mean value or a bit larger for the lowest wavenumbers. Composites are presented for each individual dataset (Fig. 4.2) and for all three datasets combined (Fig. 4.4).

The RV power spectrum shown earlier serves as our zero-order null hypothesis for a hurricane's power spectrum in the absence of turbulence. As a TC strengthens, we hypothesize that its power spectrum will approach the RV spectrum. A remarkable degree of consistency is evident between each of the composites. As storm intensity increases, spectral power increases across all scales. Spectra for all Saffir-Simpson categories exhibit a $k^{-5/3}$ spectral slope at high wavenumbers (wavelengths less than roughly 20 km) and gradually steeper slopes as the curves progress toward low wavenumbers. The scale at which steepening first occurs appears to be smaller for stronger storms. Fig. 4.3 depicts this downscale shift for the joint composite, showing that the Cat-5 power spectrum steepens between 11 and 18 km, Cat-4 between 18 and 28 km, and Cat-3 between 28 and 43 km. Initial steepening for Cat-2 and Cat-1 is somewhat ambiguous, but may be between 28 and 43 km. The TS power spectrum shows slightly elevated slopes between 43 and 166 km, but is very close to a

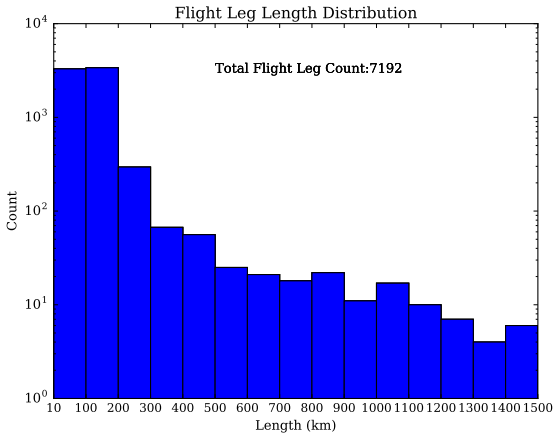

Figure 4.1: Flight leg length distribution.

$k^{-5/3}$ slope across all scales. The region of greatest power is generally found to be between 50 km and 200 km regardless of storm intensity. Although a $k^{-5/3}$ spectral slope exists at wavelengths less than roughly 20 km, the Cat-4 and Cat-5 spectra show elevated amplitudes at wavelengths less than 5 km. Fig. 4.2(a) captures this increased power, which may be connected to the exceptionally strong convective activity found in Cat-4 and Cat-5 TCs.

The steepest slope achieved by any curve is $k^{-3.1}$ as shown in Table 2.1. Mean slope and maximum slope increase with increasing storm strength. Mean slope is defined as the 4.6 km to 166 km range. A dip in the power spectra can be seen around 200 km across all 3 datasets in addition to the joint composite. It is more pronounced for stronger storms and nonexistent for the TS curve. We suspect this dip represents a return to the "background" KE spectrum at scales not influenced by TCs. This explains the flat or occasionally positive slopes (see Fig. 4.3) at low wavenumbers. At the lowest wavenumbers, the small number of samples used to produce these averages contributes to the slope variability. This is particularly apparent in the individual dataset composites (Fig. 4.2). As mentioned earlier, there are just 96 flight legs greater than 1000 km in the joint composite. With these legs spread across six intensity categories and three datasets, the large slope variability at the low wavenumbers–

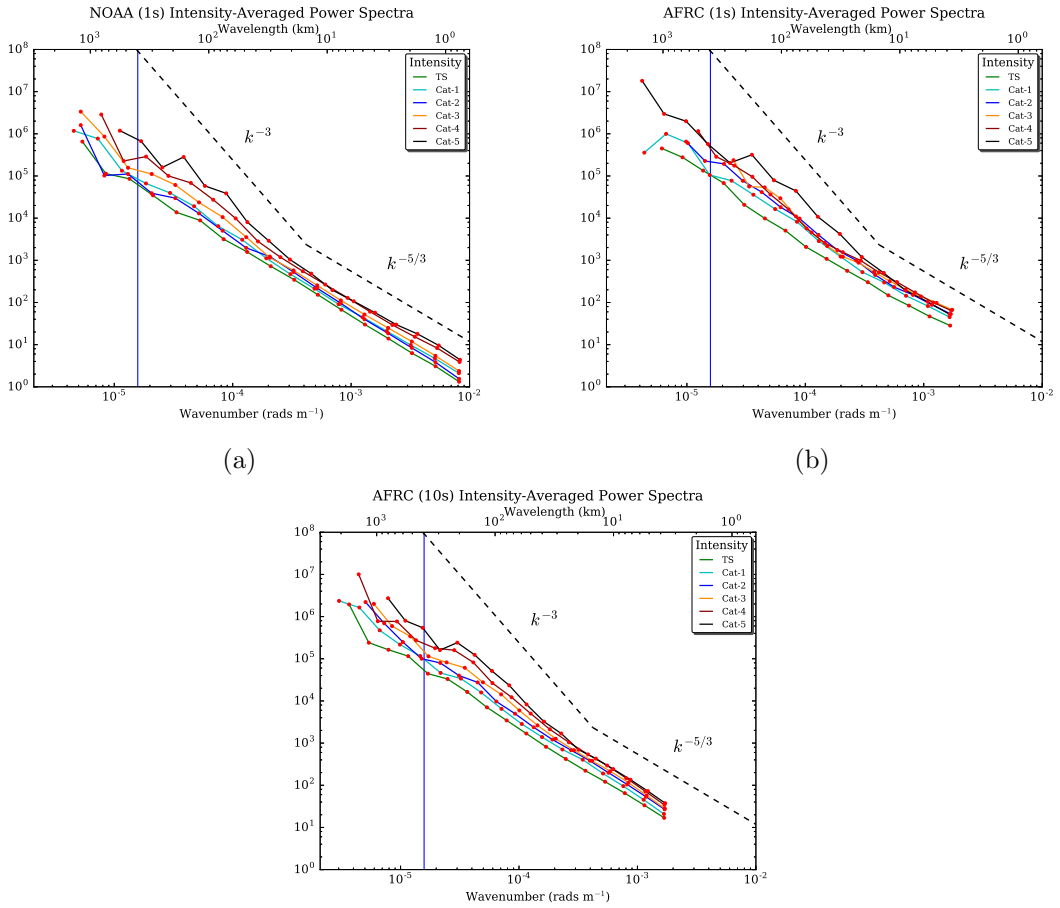

Figure 4.2: Power spectra composites for the NOAA, AFRC 1 s, and AFRC 10 s datasets color-coded by category. The blue vertical line serves as a reference for a wavelength of 400 km. Bin means–characterized by red circles– are located at the center of each bin along the x-axis. In order of sample size, the AFRC 10 s composite is comprised of the most missions (749), followed by AFRC 1 s (302), and NOAA (229).

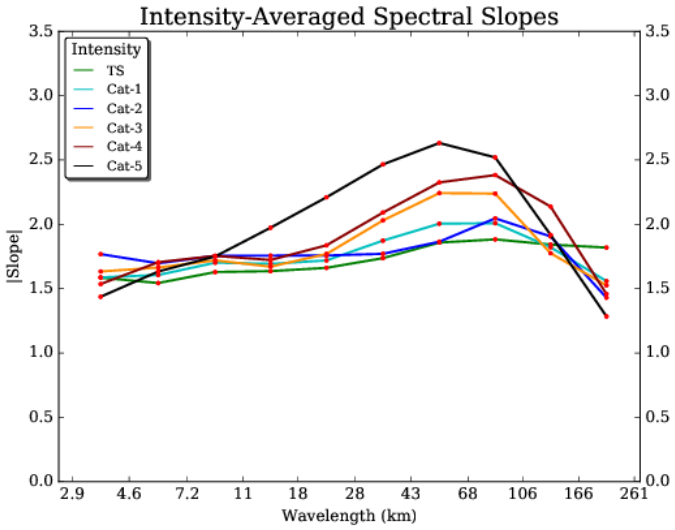

Figure 4.3: The points in this plot correspond to the bin-to-bin slopes in Fig. 4.4. From left to right, slopes vary until 2.9 km (when the NOAA data merges with the AFRC data), then gradually increase until reaching a peak slope (generally between 43 and 106 km), then decrease as the power spectrum returns to "background" levels, and finally slopes diverge at scales where few flight legs exist.

particularly for the individual composites–is not surprising. Slope variability also tends to increase with storm intensity since, naturally, the Hurricane Hunters have intercepted fewer Cat-5 hurricanes than they have Cat-1 hurricanes. For example, the AFRC 1 s composite only has 22 flight legs contributing to the Cat-5 power spectrum. Slope variability decreases at all scales for the joint composite due to the greater number of flight legs. Though we have established that the Cat-4 and Cat-5 spectra have increase power below 5 km, the apparent tightening of mean values in the joint composite at 3.1 km is an artifact of the NOAA dataset being spliced with the AFRC data as established in Section 3c.

The TS curve in the joint composite (Fig. 4.4) has mean values designated by filled black circles compared to the usual red filled circles. It serves as a reference curve for testing the difference of two means using a two-tailed z-test. Mean values displayed in red for the joint composite are found to be different than the vertically aligned reference mean at the 99% confidence level. All mean values pass this test with the exception of the Cat-1 and Cat-2 mean values at 408 km and 638 km. When calculating bin averages, values assigned to a given bin are assumed to be independent from one another. This is not strictly true considering NOAA and AFRC crews may simultaneously sample the same storm, but whenever this does happen crews make a point to sample different regions so as to avoid redundant information. On the whole, flight legs are well-diversified both spatially and temporally.

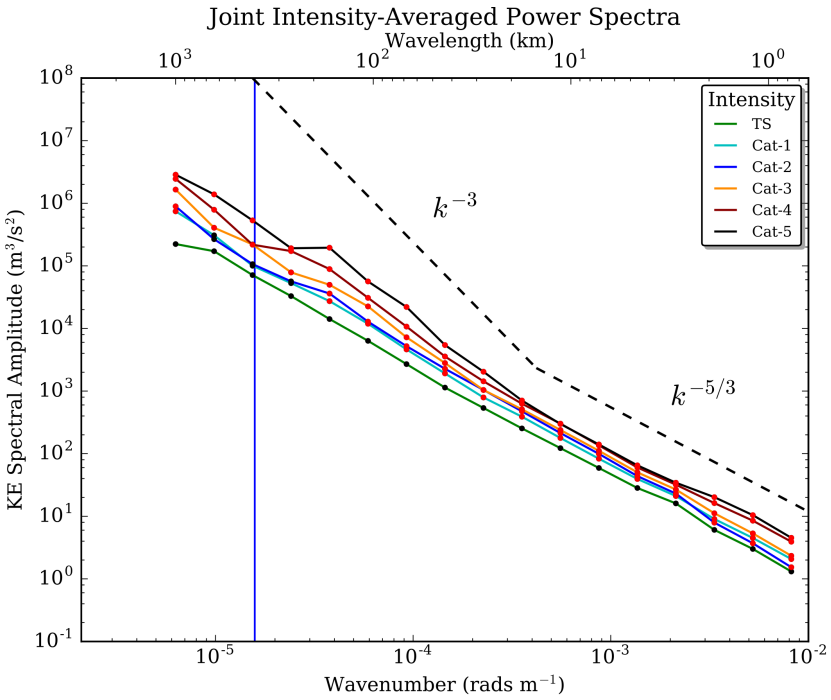

Figure 4.4: Spectral composites of all three datasets.

Chapter 5
DISCUSSION

Smith and Waleffe (1999) conducted a host of energy spectra experiments investigating the impact of rotation on spectral slope. Lindborg (2005) expanded on their work, showing that below a critical Rossby number (the limit of strong rotation) an inhibition of forward energy cascade occurs. This leads to an accumulation of energy at scales greater than the forcing scale, steepening slope. As TCs strengthen and inertial stability surges, this critical Rossby number may be achieved, causing the accumulation of energy seen over the mesoscale.

The overarching significance of spectral slope that steepens with storm intensity is that stronger storms may be more predictable than weaker storms. A modeling review conducted by Bhatia and Nolan (2013) may support this notion, having established that skill scores for the GFDL and OFCL hurricane forecasts are positively correlated with model 0-hr intensity.

Though the above hypotheses seem promising based on the natural connection to Smith and Waleffe, Lindborg, and Bhatia and Nolan's work, potential predictability implications of the power spectra composites may be thwarted by another factor. Predictability theory is grounded in flows from isotropic, homogeneous environments. A hurricane–at least flight legs along its radial cross-section–certainly violates these requirements. Could we then be sampling TC vortex structure rather than turbulent motion? Potential temperature spectra derived from the NOAA dataset suggest this may be the case (Fig. 9). If the wind spectra are representative of underlying turbulence, we would expect the potential temperature spectra to exhibit steepening with increasing temperature as well. Instead, these spectra follow an approximately $k^{-5/3}$ spectral slope with only the Cat-5 spectrum deviating from the lower intensity spectra below a wavelength of 30 km. Further research is necessary to differentiate the effects of vortex structure and turbulence on spectral slope.

Chapter 6

SUMMARY AND CONCLUSIONS

We have produced power spectra composites for each category of the Saffir-Simpson scale (including tropical storms) using data from NOAA and AFRC Hurricane Hunter missions. Over 1280 missions (7244 flight legs) were analyzed. To the best of our knowledge this is the first extensive investigation of TC power spectra using in situ aircraft data. As TC wind speeds increase, spectral slope steepens–namely over the mesoscale–and then returns to shallower levels. This return to the standard spectrum is especially apparent for the Cat-3, Cat-4, and Cat-5 composites.

Additionally, the scale at which slope begins to steepen moves downscale as storm category increases. The Cat-5 composite achieves the steepest slope of -3.1, while the TS composite only reaches a slope of -1.9. Overall, results may suggest rotation dominates TC dynamics in storms with exceptionally high wind speeds (perhaps Cat-3 and above) while stratification plays a more important role in the dynamics of weaker storms (Lindborg, 2005). If conclusions can be drawn from the spectral slopes in our composites, the idea that stronger storms are more predictable than weaker storms appears to coincide with modeling evidence put forth by Bhatia and Nolan (2013). The efficacy of these claims remains to be seen.

To examine the potential effects of rotation on TC power spectra, future work should begin with producing composites for variables such as temperature and moisture. Inspecting other variables should help settle the question as to whether power spectra are revealing information about TC structure or organic turbulence. We would also like to investigate flight paths with a constant radius from storm center. Data from these flights will have properties much closer to an isotropic, homogeneous environment. Such a study may need to be based on model data due to the rarity of missions with circular flight paths–though

they do exist. Other possible investigations include binning TCs by RMW, examining the effects of secondary eyewalls, and determining the power spectra of horizontal divergence and vertical vorticity as seen in Lindborg (2007).

BIBLIOGRAPHY

Balsley, B. B., and D. A. Carter, 1982: The spectrum of atmospheric velocity fluctuations at 8 km and 86 km. *Geophysical Research Letters*, **9**, 465468, doi:10.1029/gl009i004p00465.

Bhatia, K., and D. Nolan, 2013: Relating the skill of tropical cyclone intensity forecasts to the synoptic environment. *Wea. Forecasting*, **28**, 961980, doi:10.1175/waf-d-12-00110.1.

Chen, T.-C., and A. Wiin-Nielsen, 1978: On nonlinear cascades of atmospheric energy and enstrophy in a two-dimensional spectral index. *Tellus*, **30**, 313322, doi:10.1111/j.2153-3490.1978.tb00846.x.

Durran., D., and M. Gingrich, 2014: Atmospheric predictability: Why butterflies are not of practical importance. *J. Atmos. Sci.*, **71**, 24762488, doi:10.1175/jas-d-14-0007.1.

Durran, D., J. Weyn, and M. Menchaca, 2017: Computing dimensional spectra from gridded data and compensating for discretization errors. *Mon. Wea. Rev.*, **145**, in review.

Hsu, S., and Z. Yan, 1998: A note on the radius of maximum wind for hurricanes. *J. Coastal Res.*, **14**, 667668, doi:10.1175/waf-d-12-00110.1.

Khain, A., B. Lynn, and J. Dudhia, 2010: Aerosol effects on intensity of landfalling hurricanes as seen from simulations with the wrf model with spectral bin microphysics. *Journal of the Atmospheric Sciences*, **67**, 365384, doi:10.1175/2009jas3210.1.

Lilly, D. K., and E. L. Petersen, 1983: Aircraft measurements of atmospheric kinetic energy spectra. *Tellus*, **35A**, 379382, doi:10.3402/tellusa.v35i5.11448.

Lindborg, E., 2005: The effect of rotation on the mesoscale energy cascade in the free atmosphere. *Geophys. Res.*, **32**, L01 809, doi:10.1029/2004gl021319.

Lindborg, E., 2007: Horizontal wavenumber spectra of vertical vorticity and horizontal divergence in the upper troposphere and lower stratosphere. *J. Atmos. Sci.*, **64**, 10171025, doi:10.1175/jas3864.1.

Lorenz, E. N., 1969: The predictability of a flow which possesses many scales of motion. *Tellus*, **21**, 289307, doi:10.1111/j.2153-3490.1969.tb00444.x.

Nastrom, G. D., and K. S. Gage, 1985: A climatology of atmospheric wavenumber spectra of wind and temperature observed by commercial aircraft. *J. Atmos. Sci.*, **42 (9)**, 950960, doi:10.1175/1520-0469(1985)042¡0950:acoaws¿2.0.co;2.

National Hurricane Center, 2016: National Hurricane Center Forecast Verification: Official error trends. [Available online at http://www.nhc.noaa.gov/verification/verify5.shtml].

National Hurricane Operations Plan, 2017: NOAA Tech. Rep. FCM-P12-2016, NOAA, Silver Spring, MD, 167 pp.

Rogers, R., P. Reasor, and S. Lorsolo, 2013: Airborne doppler observations of the inner-core structural differences between intensifying and steady-state tropical cyclones. *Mon. Wea. Rev.*, **141**, 29702991, doi:10.1175/mwr-d-12-00357.1.

Rosenfeld, D., M. Clavner, and R. Nirel, 2011: Pollution and dust aerosols modulating tropical cyclones intensities. *Atmospheric Research*, **102**, 6676, doi: 10.1016/j.atmosres.2011.06.006.

Rosenfeld, D., A. Khain, B. Lynn, and W. L. Woodley, 2007: Simulation of hurricane response to suppression of warm rain by sub-micron aerosols. *Atmospheric Chemistry and Physics*, **7**, 34113424, doi:10.5194/acp-7-3411-2007.

Rotunno, R., and C. Snyder, 2008: A generalization of lorenzs model for the predictability of flows with many scales of motion. *J. Atmos. Sci.*, **65**, 10631076, doi:10.1175/2007jas2449.1.

Smith, L., and F. Waleffe, 1999: Transfer of energy to two-dimensional large scales in forced, rotating three-dimensional turbulence. *Phys. Fluids*, **11**, 16081622, doi:10.1063/1.870022.

Vinnichenko, N. K., 1970: The kinetic energy spectrum in the free atmosphere-1 second to 5 years. *Tellus*, **22**, 158166, doi:10.1111/j.2153-3490.1970.tb01517.x.

Weather Bird Software Logic and Algorithms, 2016: [Available directly through the 53 Weather Reconnaissance Squadron].

Appendix A

STANDARD OPERATING PROCEDURES AND DATA QUALITY

A.1 Aircrew Standard Operating Procedures

Each storm intercept is complimented by a corresponding mission summary and accompanying radar data. Flight tracks generally resemble a "Figure 4" over investigated storms, with intercepting flight legs oriented along intercardinal (45°, 135°, 225°, 315°) directions. Once crews have committed to an intercept, every effort is made to maintain a straight flight path and consistent speed through the RMW (National Hurricane Operations Plan). Flights are executed along a 925 millibar (mb), 850 mb, or 700 mb pressure surface depending on whether the target storm is a tropical invest, tropical depression/storm, or hurricane (National Hurricane Operations Plan). Flight leg length varies based on storm diameter and customer priorities, but 96% of legs used in this study are 300 km or less. Recorded variables and aircraft type have fluctuated over the half century hurricane hunting operations have transpired, but they remain fairly consistent from decade to decade. Official mission data dates back to Hurricane Donna in 1960, but the U.S. Navy and the U.S. Weather Bureau conducted flights even earlier. More detail about the NOAA and AFRC Hurricane Hunters standard operating procedures can be found in the publicly available National Hurricane Operations Plan.

A.2 NOAA and AFRC Data Quality

As a form of quality control, software managing the AFRC 10 s data requires a minimum of 7 data points to be present in a given 10 s period for a 10 s average to be recorded. If less than 7 data points are available to contribute to the 10 s average, that line is coded as

missing data. In the AFRC 1 s dataset, 10 data points must be present in order for a 30 s average to be valid. NOAA data was either present or missing for a given second with no specified quality control measures. Further detail about AFRC data quality can be found in the Weather Bird Software Logic and Algorithms manual (available through the 53WRS).

Missing data was rare: roughly 1 in 190 observations for the NOAA and AFRC 1 s data, and 1 in 355 observations for the AFRC 10 s data. Spectral analysis was performed on all flight legs regardless of missing data and then only performed on flight legs with no missing data. Results varied negligibly, so all available flight legs were utilized. Outliers caused by instrument error were only present in flight data from Hurricane Allen (1980) and Hurricane Gilbert (1988). These outliers were removed before analysis.